



## Research Article

# Short alkyl chain length ionic liquid as organic modifier in polypropylene/clay nanocomposite: a thermal comparative study

Priscila Vedovello<sup>1</sup>  · Ana Catarina de Oliveira Gomes<sup>2</sup>  · Lucas Mendonça da Rocha Oliveira<sup>1</sup>  · Sandra Andrea Cruz<sup>1</sup>  · Caio Marcio Paranhos<sup>1</sup> 

Received: 18 November 2020 / Accepted: 10 April 2021

Published online: 23 April 2021

@ The Author(s) 2021 

## Abstract

The most common polymeric nanocomposites are constituted of organically-modified clays. Generally, these organic modifiers are based on quaternary ammonium salts. These systems have as disadvantage the low thermal resistance of its modifiers under processing. Ionic liquids (IL) with different molecular structures can be used as organic modifier in lamellar clays-based polymeric nanocomposites, being promising not only to increase interactions between the nanoclay and the matrix, but also to increase the thermal resistance. In this study, polypropylene-based/montmorillonite nanocomposites were compared from two different organic modifiers. The use of short alkyl chain length imidazolium-based IL as montmorillonite modifier was investigated in terms of the thermal stability when compared to the usual quaternary ammonium salt surfactant. Integral procedure decomposition temperature was employed to determine the effect of these two different organoclay modifiers in PP-nanocomposites. The activation energy for these samples was calculated using Flynn–Wall–Ozawa (FWO) method. It was also used the multiple linear regression analysis to calculate the activation energy in order to evaluate the accuracy of this method when applied to nanocomposites.

## Article Highlights

- Short length alkyl group in ionic liquid was able to improve the thermal stability of PP-based nanocomposite.
- IPDT methodology is more realistic to evaluate the thermal stability of ionic liquid-based nanocomposite.
- MLR methodology was efficient to assess the entropic contribution associated to polymer-clay interactions, inter-lamellae spaces and interface morphology.

**Keywords** Ionic liquid · Polypropylene · Nanocomposite · Thermal stability

**Supplementary Information** The online version contains supplementary material available at <https://doi.org/10.1007/s42452-021-04573-w>.

✉ Caio Marcio Paranhos, [paranhos@ufscar.br](mailto:paranhos@ufscar.br) | <sup>1</sup>Polymer Laboratory, Department of Chemistry, Federal University of Sao Carlos, Rod. Washington Luiz, km 235, Sao Carlos, SP CEP 13565-905, Brazil. <sup>2</sup>SENAI Innovation Institute for Green Chemistry, Rua Moraes E Silva, 53, Bd 09, Rio de Janeiro, RJ CEP 20271-030, Brazil.



SN Applied Sciences (2021) 3:579 | <https://doi.org/10.1007/s42452-021-04573-w>

## 1 Introduction

Nanocomposites based on organically modified clays especially montmorillonite (MMT) have been attracting great interest to be used in polymeric matrices due to significant influences on the mechanical properties, gases and liquids permeability, barrier properties and thermal resistance [1–5]. It is well established that the presence of nano-sized inorganic particles into polymeric matrices may result in significant changes on the final properties of these materials when compared to the traditional polymeric composites [6]. The most common polymeric nanocomposites are constituted by organically-modified clays as nanofillers. Several authors have reported the use of organically-based modifiers in order to improve the chemical affinity between the inorganic (clay—hydrophilic) and the organic (polymer—hydrophobic) phases [6, 7]. This key-factor is more relevant in the case of polyolefins, as polyethylene (PE) and polypropylene (PP), which are unfavorable thermodynamically for the nanodispersion of inorganic clay layers in the polymer matrix, because of the incompatibility of hydrophobic polyolefin and hydrophilic clay [8, 9]. To obtain a successful preparation of polyolefin-based nanocomposites, ions can be exchanged by a wide variety of hydrated inorganic or organic cations, including those of amines, quaternary ammonium salts or alkylphosphonium cations [3, 5, 7, 10–13].

It is well-known that the miscibility between layered clay nanoparticles and olefins polymers is low. Cationic surfactants are used to increase the hydrophobicity of the clay surfaces by ion-exchange reactions [6]. Alkylammonium cations are widely used to clay surfactants in different layered clay, as montmorillonite [7]. However clay surfactants based on quaternary ammonium salts have as disadvantage the low thermal resistance when submitted to high processing temperatures [14, 15]. As a matter of fact, quaternary ammonium salts start its thermal decomposition at ~ 180 °C [12, 16]. Several polymers as polyolefins and engineering polymers, such as polyamides and polyesters, show higher processing temperatures than the onset decomposition temperature of the surfactants. Some new approaches to overcome the thermal limitation of the clay modifiers under processing were investigated. Studies lead by Ngo and co-authors has demonstrated the elevated thermal resistance of imidazolium-based ionic liquids (IL) [17]. The use of IL with different molecular structures, as organic modifier in polymeric nanocomposites based on lamellar clays, is promissory not only to increase the interaction between the nanoclay and the matrix, but also to present the thermal resistance superior to those of the traditional surfactants. IL offer some interesting advantages as easy handling, high thermal stability, and

capacity to form stable organic ions and counter-ions. The IL acting as modifiers in polystyrene and polyamide/poly-carbonate nanocomposites was investigated by Zhu et al. [18] and Cui et al. [19], respectively. The authors concluded that the IL are more thermally stable when compared to the conventional quaternary ammonium salts. Despite the fact that the use of IL is a well-known strategy to improve the chemical affinity between clay–polymer phases, few investigations addressed the comparative aspects of thermal stability of IL and MMT. In addition, how the effect of the alkyl length in IL on the thermal stability of polymeric nanocomposites when compared to the traditional quaternary ammonium salts remains as an important question.

In this investigation, organoclays based on IL obtained from the modification of 1,2-dimethyl imidazole was prepared. The main objective was to evaluate the use of IL with short alkyl chain length as clay modifier and to compare to the conventional quaternary ammonium surfactant in PP-based nanocomposites. Systematic evaluation of the thermal stability of the samples was conducted using non-conventional methodology, as integral procedure decomposition temperature (IPDT) and multiple linear regression (MLR) differential method.

## 2 Experimental

### 2.1 Synthesis of 1-butyl-2,3-dimethylimidazolium chloride [BMMIM]Cl

The synthesis of 1-butyl-2,3-dimethylimidazolium chloride [BMMIM]Cl (Fig. 1) was based on the work of Cammarata [20].

Basically, 1,2-dimethyl imidazoline (Sigma-Aldrich) was added to toluene (Synth) at 0°C under vigorous stirring and then 1-chlorobutane (Sigma-Aldrich) was added. Additionally, the solution was maintained for 24 h at 110 °C under reflux. The obtained solution was kept in a freezer at ca. – 12 °C for 12 h. The purification of [BMMIM]Cl was performed using toluene, acetonitrile, and ethyl acetate [20]. The NMR spectra were obtained at room temperature on a Bruker Advance 400 spectrometer. The measures of <sup>13</sup>C NMR were performed at 100 MHz, using deuterated water (D<sub>2</sub>O) as a solvent and the measures <sup>1</sup>H NMR were performed at 400 MHz using deuterated chloroform (CDCl<sub>3</sub>) as the solvent. The chemical shifts were calculated from the internal standard TMS (tetramethylsilane). The NMR spectra are shown in Figs S1 and S2. The chemical shifts observed for <sup>1</sup>H NMR and <sup>13</sup>C NMR spectra of [BMMIM]Cl are in agreement with values reported by Dupont [21]. In <sup>13</sup>C NMR was obtained shifts around 17.9; 30.2; 34.1; 46.8; 119.8; 121.5 and 141.9 ppm. In <sup>1</sup>H NMR the shifts were 0.95 (t, 3H); 1.35 (m, 2H); 1.8 (m, 2H); 4.04 (s, 3H); 4.28 (t, 2H)

and 7.7 (s, 1H) ppm. Differences observed for displacement of CH<sub>2</sub>-region is possibly due to the presence of chloride counter-ion, as reported by Xu and co-authors [22]. From the results, the IL synthesis yielded 75%.

## 2.2 Preparation of PP-based nanocomposites

The organoclays were obtained by direct swelling of the natural clay in the IL (MMT-IL). MMT clay (MMT-Na<sup>+</sup> Coisite<sup>®</sup>), named in this work as MMT, was added in deionized water under vigorous stirring at 70 °C for 12 h. [BMMIM]Cl (1:5 wt% IL-clay ratio) was added and stirred for 3 h. The organophilic clay was dried under vacuum at 60 °C for 24 h. MMT containing quaternary ammonium salt as clay surfactant (Cloisite 20A<sup>®</sup>) were used and supplied by Southern Clay Products. It is named as MMT-20A.

PP (H501C) with a melt flow index of 3.5 g/10 min, was kindly provided by Braskem. PP grafted with maleic anhydride (PP-*g*-MAH, 0.5 mol % of MAH, OREVAC 100 supplied by Arkema) was used as compatibilizer. PP/PP-*g*-MAH/organoclay nanocomposites (95.5/4.5/1.5, 85/9/3 and 80/15/5 ratios) were prepared by using a high shear thermokinetic mixer (Drais) at 3000 rpm for 1.5 min. The mixer was fed by all components simultaneously. For comparison purposes, nanocomposites containing MMT-20A clay were prepared using the same protocol.

## 2.3 Characterization

The dispersion and intercalation of PP melt into the clay layers was studied by transmission electron microscopy (TEM). TEM images of the nanocomposites were taken at room temperature. The TEM grids were mounted in liquid nitrogen cooled sample holder. The ultrathin sectioning (40–60 nm) was performed by ultramicrotomy at low temperature using a Reichert Ultracut FC S low temperature sectioning system. A transmission electron microscope (Fei Tecnai G<sup>2</sup> F20 HRTEM) operated at 80 kV was used to obtain images of the nanocomposite specimens. Wide angle X-ray scattering diffraction measurement (WAXS) was performed in a Shimadzu XRD6000 in a 2θ range of

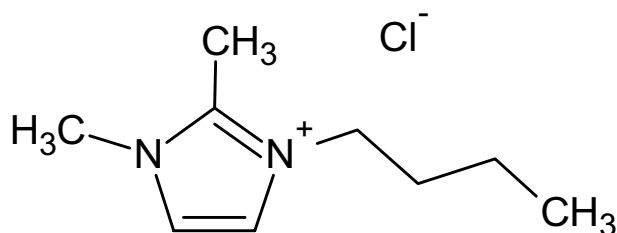


Fig. 1 Chemical structure of [BMMIM]Cl

2–40° at room temperature, operating under a CuKα radiation ( $\lambda = 1.5405 \text{ \AA}$ ). The infrared spectra of the samples were recorded by Varian Excalibur 3100 FTIR-ATR. Samples were placed in direct contact with the ZnSe crystal. Spectra were collected with  $2 \text{ cm}^{-1}$  spectral resolution and twenty scans were performed for each sample. The thermogravimetric curves (TGA) of the samples were obtained by an equipment of TA Instruments TGA Q50. Samples (~5.0 mg) were placed in platinum crucibles. Four different heating rates were used (5, 10, 20, and  $40 \text{ }^\circ\text{C}\cdot\text{min}^{-1}$ ) under an inert atmosphere of nitrogen (40 mL/min), at the temperature range of 30–800 °C.

## 3 Results and discussion

### 3.1 Characterization of pristine and modified MMT

Figure 2 shows the WAXS patterns of the pristine MMT clay and the organically-modified MMT-20A and MMT-IL clays. MMT shows a diffraction peak at  $2\theta = 7.22^\circ$ , corresponding to a d spacing = 12.2 Å. The presence of the surfactants resulted in a shift of this diffraction peak towards smaller angles ( $2\theta = 4.51^\circ$  and  $2\theta = 3.60^\circ$  for MMT-IL and MMT-20A, respectively), which corresponds to a d spacing of 19.6 Å and 24.5 Å. These values suggest a degree of intercalation of the surfactants into the pristine MMT galleries. Due to its molecular volume the quaternary ammonium salt present in MMT-20A clay contributes to increase the d spacing of the clay galleries when compared to the [BMMIM]Cl modifier present in MMT-IL clay.

The FTIR spectra obtained for the pristine MMT and organically modified clays are shown in Fig. 3. The broad absorption band near  $3440 \text{ cm}^{-1}$  and the strong peak at  $1640 \text{ cm}^{-1}$  are representative of the stretching and bending modes of absorbed water. Hydroxyl groups stretching corresponds to the broad shoulder centered at  $3430 \text{ cm}^{-1}$ . Si–O bonds were observed at  $1040 \text{ cm}^{-1}$ . Incorporation of the organic modifiers into the pristine clay was confirmed by bands at  $1460$  and  $1375 \text{ cm}^{-1}$  (–CH<sub>2</sub>– and –C–CH<sub>3</sub> stretching, respectively) and  $720 \text{ cm}^{-1}$  (–C–N–stretching). However, there are some bands in MMT-IL spectrum, which are not exhibited by the MMT-20A sample. Located at  $1540$ – $1600 \text{ cm}^{-1}$ , these bands are assigned to C–N–C and C–C bonds from imidazolium group [23]. Also, it seems that [BMMIM]Cl modifier alter water absorption into the clay, since the intensity of the  $3440 \text{ cm}^{-1}$  and  $1640 \text{ cm}^{-1}$  bands diminishes.

Figure 4 shows the TGA curves mass loss as well as the first derivative curves obtained for MMT, MMT-IL and MMT-20A. The evaluation of degradative processes will be described in this work in two aspects: (1) evaluation of the maximum speed mass loss temperature ( $T_{\text{max}}$ ),

determined by the maximum value of the first derivative and (2) the intensity of the first derivative of percentage mass loss, which is related to the amount of mass loss in each of the processes. Therefore, it could be observed that the pristine MMT presents two different mass loss processes. One of them more intense with  $T_{\max}$  42 °C and other one in 640 °C. These processes are respectively attributed to desorption of water and to the dehydroxylation of the clay [24]. The first process is not observed to the modified clay, since the modifier alters water absorption into the clay, as verified by the FTIR results.

For MMT-20A there are three mass loss processes that occur in 314, 407 and 580 °C approximately, as can be seen in Fig. 4. The two first processes that occur in lower temperatures (314 and 407 °C) overlap. This suggests that the first one is related to physically bond modifier in the clay surface and the higher one is related to the alkyl ammonium intercalated in the clay galleries. These are the processes with higher mass loss, as could be clearly visualised by the higher intensity of the first derivative peak between 180 and 480 °C. At these temperatures occur decomposition reactions of alkyl ammonium salts by Hoffmann elimination reaction. As described by Lima and co-workers [25] in a study about MMT incorporated in low molar mass PET, the elimination occurs by the extraction of a hydrogen atom from C-tallow structure of the salt quaternary ammonium. As a result, there is an olefinic and a tertiary amine groups, as described in Fig. 5.

The third peak (580 °C) refers to dehydroxylation of the clay and it was shifted to lower temperatures when compared to pristine MMT. Hoffman elimination reaction produces a hydrogen proton in the clays surface which should be acting as the acidic sites to accelerate the dehydroxylation and consequently reducing the temperature of this process [26].

The MMT-IL presents three well-defined processes of mass loss in  $T_{\max}$  as 314, 495 and 582 °C. The pure IL presents a decomposition that occurs majoritarily in one-step (Fig. S3) at the range of 230–350 °C. There is a significant increase in mass loss temperature, which could be related to the strong interactions between IL and clay. The first peak of MMT-IL was attributed, as previously described, to the species physically adsorbed on the MMT surface. On the other hand, well-intercalated IL presents the mass loss peak observed at 495 °C. This statement could be confirmed by the X-rays results and the same behavior could also be verified to MMT-20A (Fig. 2).

The MMT and the modified MMT show approximately by 85 and 40% of the residue indicating that this clay is partially composed by inorganic materials as metallic oxides. In general, the residues do not play a key role in the thermal degradation of organoclays. However, it is important to emphasize that the residual metal specimens could, together with high temperatures, have favored the degradation process of polymer matrix. The catalysts used in the polymerization, as well as the processing step are

**Fig. 2** WAXS patterns of pristine MMT- $\text{Na}^+$  and organically modified MMT clays

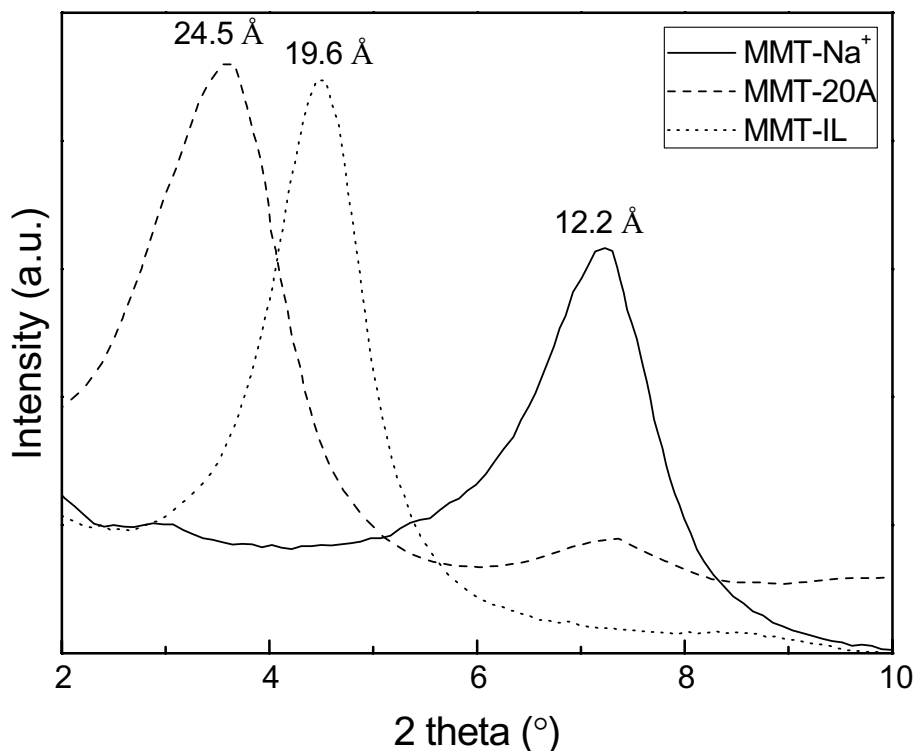


**Fig. 3** FTIR spectra of pristine MMT and organically modified MMT samples

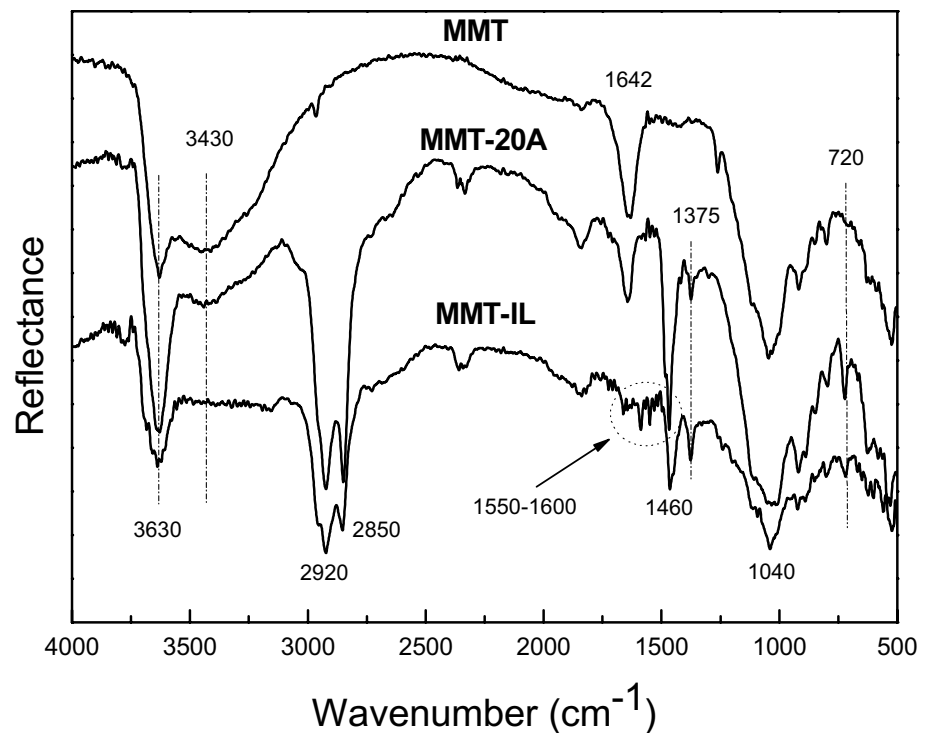
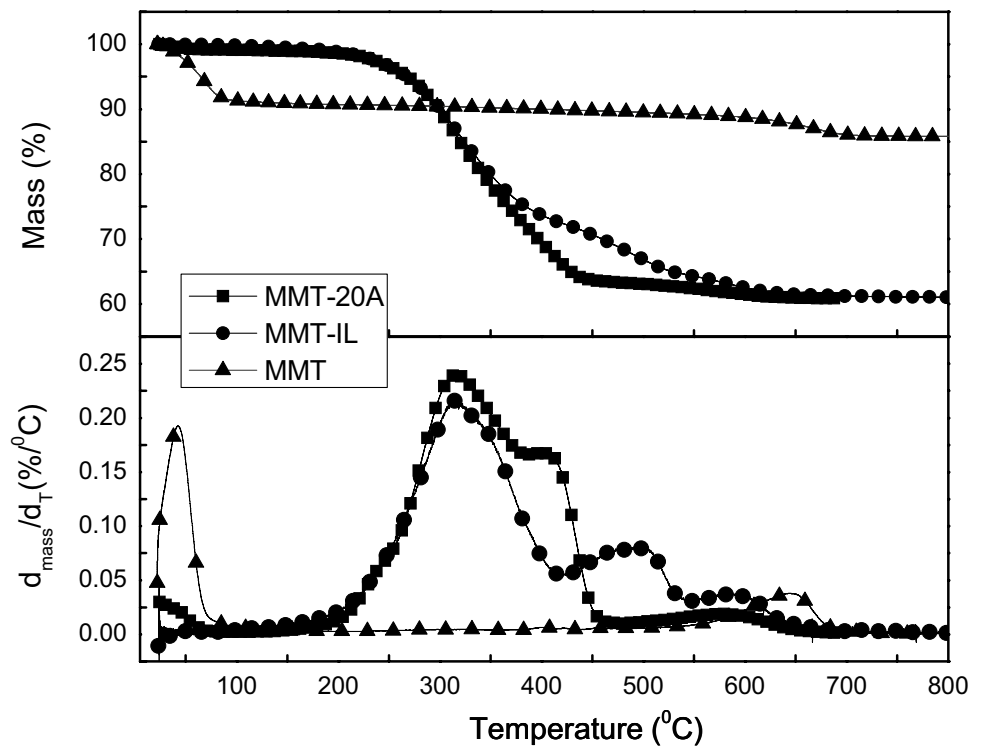


**Fig. 4** Thermogravimetric curves and the first derivative curves for the MMT-20A, MMT-IL and pristine MMT *HT*—hydrogenated tallow with ~65% C18, ~30% C16, ~5% C14



metallic sources. In nanocomposites based on clays there are an additional issue due to the metal presents in its structure [27]. Besides, the presence of oxygen and the metal specimens may act as catalyst to cleavage of alkenes

from salt quaternary ammonium to produce aldehydes at elevated temperature [12].

### 3.2 Thermal stability of nanocomposites

In order to evaluate the thermal stability of the nanocomposites it was used the IPDT proposed by Doyle [28]. As previously described, it is necessary to guarantee the thermal stability of the surfactants in terms of the processing temperature. Thus, IPDT seems to be more realistic to evaluate the performance of these two organoclays, since the IPDT protocol take into account the volatile fraction of the polymeric matrix under decomposition and may be used to estimate the inherent thermal stability of the nanocomposites. Taking this aspect into account, we adopted a higher heating rate ( $40\text{ }^{\circ}\text{C}\cdot\text{min}^{-1}$ ) than the usually used in decomposition kinetics studies. IPDT may be calculated from:

$$IPDT = A \cdot K(T_f - T_i) + T_i \quad (1)$$

$$A = \frac{S_1 + S_2}{S_1 + S_2 + S_3} \quad (2)$$

$$K = \frac{S_1 + S_2}{S_1} \quad (3)$$

where  $A$  is the area ratio of total experimental TGA curve and  $T_i$  and  $T_f$  are the initial and final experimental temperatures, respectively. The terms  $S$  and  $K$  are geometrical factors obtained from a graphical procedure on the TGA curves, as showed in Fig. 6 [28].

Table 1 summarizes the values of IPDT and the maximum decomposition temperature ( $T_{\text{max}}$ ) obtained from the maximum value of the first derivative TGA curve of the nanocomposites.

For all clay content studied in this investigation organoclays based on IL showed  $T_{\text{max}}$  values higher than 20A organoclays. In terms of IPDT, the performance of these organoclays is even more remarkable. Thus, the incorporation of [BMMIM]Cl IL as modifier for MMT improved the thermal stability of PP-based nanocomposites

significantly. Awad and co-authors have attributed the high thermal stability of imidazolium-based IL to the partial cleavage of the IL via  $S_N2$  process [14]. It seems that the  $S_N2$  process does not contribute to open the imidazolium ring and, therefore, maintain the structure of the IL at elevated temperatures. Depending on the alkyl chain of the quaternary ammonium salts, the decomposition process can take place via  $S_N1$  or  $S_N2$  mechanism. Moreover, the pyrolysis products are obviously less stable than the imidazolium ring. In addition, it is known that the thermal behavior is strongly dependent of many factors as interface morphology, inter-lamellar distance, and the amount of free volume. The geometric constrain imposed by the intercalated and exfoliated structures results in an increase in the mean free path to the output volatiles. This feature delay initiation and evolution of the loss volatiles.

Differing from the conventional TGA analysis, IPDT procedure considers the area under TGA curve. The obtained area is normalized by the experimental temperature range. The product  $A \cdot K$  incorporate two contributions: the final volatilization temperature and the refractoriness of the nanocomposite components. Since materials with high refractoriness can initiate its thermal decomposition at lower temperatures, this behavior is not considered in conventional TGA. Consequently, IPDT can be understood as a half-volatilization temperature normalized by the experimental temperature range and more realistic when compared to standard  $T_{50}$  (temperature at which 50% of the polymer mass are lost). Moreover, the reproducibility of the IPDT results are more robust than the conventional TGA, even performed at different heating rates.

The thermal behavior of the clay surfactants/modifiers in the nanocomposites is an important issue to increase the applicability of polymeric materials. The results show the IL presents two positive aspects as compared to quaternary ammonium salts: (1) a higher thermal stability and (2) an improvement in the intercalation as required to make a nanocomposite with good properties. Therefore,



*HT* = hydrogenated tallow with ~65% C18, ~30% C16, ~5% C14

Fig. 5 The Hoffman elimination reaction for quaternary ammonium compounds in organoclays

the kinetics of thermal degradation study was done for the IL based-nanocomposites.

### 3.3 Kinetics of thermal degradation

Kinetic analysis of thermal degradation for the IL nanocomposites was performed by the Flynn–Wall–Ozawa (FWO) method [29, 30]. This method is classified as an integral method and the activation energy can be determined from mass loss versus temperature at different heating rates directly [31]. Kinetic studies were based on the general equation at which decomposition rate  $d\alpha/dt$  depends on the temperature and mass of the sample:

$$\frac{d\alpha}{dt} = k(T)f(\alpha) \tag{4}$$

where  $k$  is the kinetic constant and  $f(\alpha)$  is a function of the conversion, and the degree of conversion ( $\alpha$ ) was determined by:

$$\alpha = \frac{m_0 - m}{m_0 - m_\infty} \tag{5}$$

where  $m$  is the mass at temperature  $T$ ,  $m_0$  is the initial mass of the sample and  $m_\infty$  is the residual mass at the end of the experiment. The temperature depends on the kinetic constant ( $k$ ) which can be given by the Arrhenius-type:

**Table 1** Integral procedure decomposition temperature (IPDT) and maximum decomposition temperature ( $T_{max}$ ) obtained by the PP-based nanocomposites at  $10\text{ }^\circ\text{C}\cdot\text{min}^{-1}$

Content of organoclay (wt%)	Quaternary ammonium salt		[BMMIM]Cl	
	IPDT ( $^\circ\text{C}$ )	$T_{max}$ ( $^\circ\text{C}$ )	IPDT ( $^\circ\text{C}$ )	$T_{max}$ ( $^\circ\text{C}$ )
1.5	456	437	503	468
3.0	465	440	553	469
5.0	458	445	549	460

Experimental IPDT and  $T_{max}$  from pure PP are  $474\text{ }^\circ\text{C}$  and  $452\text{ }^\circ\text{C}$ , respectively. The confidence limit was fixed in the range of  $\pm 5\%$

$$k(T) = Ae^{\left(\frac{-E_a}{RT}\right)} \tag{6}$$

where  $A$  is a pre-exponential factor ( $\text{min}^{-1}$ ),  $E_a$  is the activation energy for the decomposition process ( $\text{J mol}^{-1}$ ),  $R$  is the constant of gases ( $8.314\text{ J K}^{-1}\text{ mol}^{-1}$ ),  $T$  is the temperature (K). If:

$$f(\alpha) = (1 - \alpha)^n \tag{7}$$

then combining the Eqs. (4-7) Eq. (4) can be rewritten as follows:

$$\frac{d\alpha}{dt} = A \exp\left(\frac{-E_a}{RT}\right)(1 - \alpha)^n \tag{8}$$

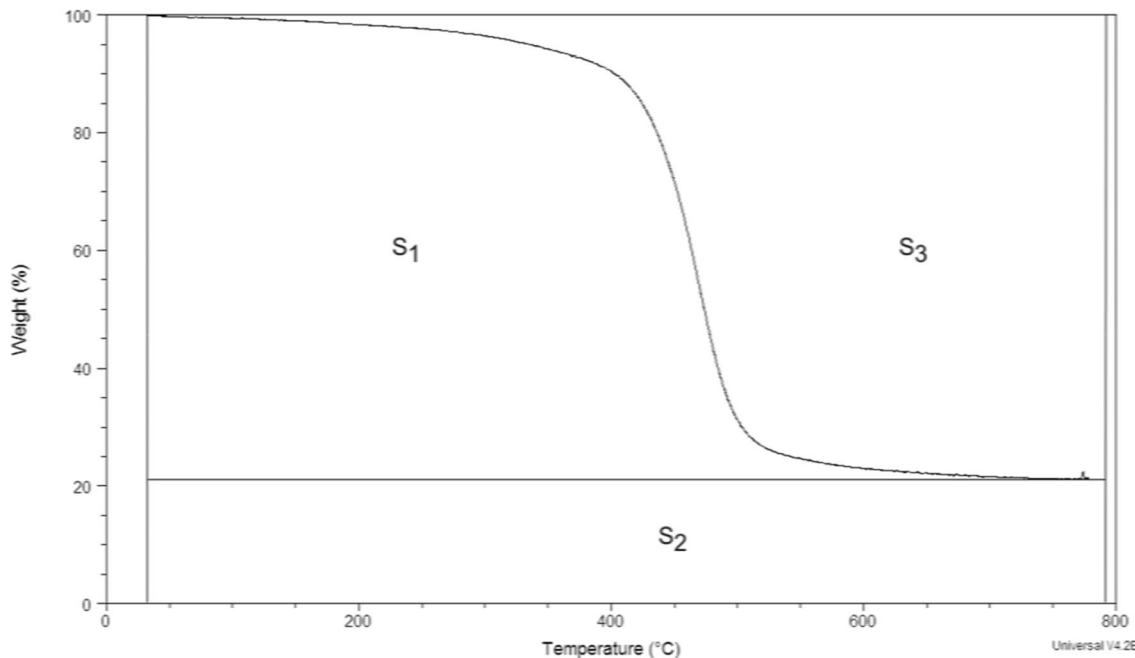


**Fig. 6** Graphical procedure to determine the IPDT

where  $n$  is the reaction order. A differential Eq. (8) can be manipulated resulting in a straight line for kinetic parameters to be obtained from the slope. Among all linear forms of Eq. (8), the Ozawa's method is widely used. The decomposition curves of samples at different heating rates ( $\beta$ ) lead to the following relation:

$$\frac{d\alpha}{(1-\alpha)^n} = \left[ \frac{Ae^{(-E_a/RT)}}{\beta} \right] dt \tag{9}$$

where  $\beta$ =heating rate. FWO method considers several TGA curves obtained at various heating rates.

The differential Eq. (9) can be simplified using Doyle's approximation [32]:

$$\ln \beta = \ln \left( \frac{AE_a}{R} \right) - 5.3305 - 1.0516 \frac{E}{RT} - \ln F(\alpha) \tag{10}$$

where  $F(\alpha)$  is an expansion by power series resulting from the integration of the exponential term. Consequently, for constant values of conversion degrees, curves of  $\ln \beta$  versus  $1/T$ , obtained at different heating rates, will result in straight lines with an approximate coefficient of  $-1.0156 (E_a/R)$ .

The order of the decomposition reaction was estimated by the modified- Kissinger method, as proposed by Carrasco et al. [33], taking into account the area of the second derivative of the  $\alpha$  vs.  $T$  curves:

$$n = \frac{\int_{T_i(\alpha=0)}^{T_m} \left( \frac{\partial^2 \alpha}{\partial T^2} \right)_{1stpeak} dT}{\int_{T_m}^{T_f(\alpha=1)} \left( \frac{\partial^2 \alpha}{\partial T^2} \right)_{2ndpeak} dT} \tag{11}$$

Table 2 shows the activation energy of pure PP and PP-based nanocomposites with different content of MMT-IL in degree of conversion ( $\alpha$ ) range of 5–20%.

It is interesting to note that the order of magnitude of the  $E_a$  data obtained by the FWO method agree with the data reported by Nisar and co-authors for PP. According to Nisar, the  $E_a$  values have a strong relation to the degree of conversion. As  $\alpha$  increases, the activation energy also increases, indicating that the degradation of PP occurs in multiple stages, through a series of consecutive or competitive reactions [34].

Activation energy values during the thermal degradation of the composites decrease with the increase of the incorporated MMT-IL concentration, except for the 3.0 wt.% MMT-IL sample. This behavior can be related to a better dispersion obtained, in this content, with several regions with lamellae of clay intercalated and exfoliated. The morphology of nanocomposites was observed via TEM as shown in Fig. 7. The entropic contribution was associated to polymer–clay interactions, inter-lamellae

spaces and interface morphology. Moreover, complex dynamics in the polymer/layered clay nanocomposites can occur due to the geometric constraint imposed by the two-dimensional space of the intercalated and exfoliated clays. It is possible to notice the presence of small tactoids of MMT. Increasing the content of MMT to 3.0 wt% (Fig. 7c) resulted in several regions with intercalated lamellae and exfoliated, indicating a better dispersion of the clay into the polymer matrix. For 5.0 wt% MMT-IL the modified clay shows morphology similar to that observed for the composition of 1.5 wt% MMT-IL nanocomposite but with more compact and deformed tactoids reducing the exfoliation degree. In this way the degree of intercalation/exfoliation could be related to the enthalpy component ( $\Delta H = E_a - RT$ ) which results in higher activation energy, as can be seen in Table 2. This statement could be also confirmed with the higher IPDT values observed to these samples, as showed in Table 1.

The global data obtained by the FWO method is qualitative in relation to the observed thermal decomposition. Apparently, it has a perception that the PP is more thermally stable than the samples with 1.5 and 5 wt% MMT-IL, due to higher  $E_a$ . However, the model cannot predict the individual contribution of polymer matrix and modifier on the simultaneous mechanisms of decomposition.

An interesting technique for the quantitative determination of the data obtained via non-isothermal methods by TGA or DSC was proposed by Widmann [35]. The differential Eq. (8) can be written in logarithmic form to obtain the multiple linear equation of the type:

$$\ln \left( \frac{d\alpha}{dt} \right) = \ln A + E_a \left( \frac{1}{-RT} \right) + n \ln (1 - \alpha) \tag{12}$$

The MLR analysis (Eq. 13) provides the kinetic data through a single 3D plot from the measurements of the thermoanalytical curve (Fig. S4). Table 3 shows the parameters provided by the thermal degradation kinetic study conducted by the MLR method.

**Table 2** Thermal decomposition parameters obtained by FWO method in the  $\alpha$  range 5–20% for PP/MMT-IL nanocomposites

Content of organoclay (wt%)	$E_a$ (kJ.mol <sup>-1</sup> )			Reaction order ( $n$ )
	$\alpha=5\%$	$\alpha=10\%$	$\alpha=20\%$	
0.0	164.72	168.40	171.63	1.00
1.5	155.22	169.55	178.92	1.00
3.0	196.83	209.66	207.70	1.00
5.0	128.29	148.13	164.81	0.98

The confidence limit was fixed in the range of  $\pm 5\%$

According to the data obtained by the MLR method, the order of reactions for the decomposition of all materials with different concentrations of modifiers were  $\leq 1$ , as predicted in the FWO method. However, the  $E_a$  values obtained are significantly higher than those obtained by FWO. High  $E_a$  value ( $328 \text{ kJ}\cdot\text{mol}^{-1}$ ) for PP was previously reported by Chan and Balke [36]. These authors showed that PP decomposes thermally in three different regions associated to a range. Higher  $\alpha$  values correspond to higher  $E_a$ . On the other hand, it is well established that the thermal decomposition mechanism of PP and other polyolefins changes in a narrow  $\alpha$  range, including the effect of autocatalysis [34, 37, 38]. MLR method considers a wide range of  $\alpha$  (0.1–0.8) to calculate the thermal parameters [35, 39]. It seems that MLR method is more

inaccurate to predict the  $E_a$  values for polyolefins as PP. However, it is interesting to note that the average  $E_a$  remain below the value of pure PP, except for the nanocomposite containing 3.0 wt.% of clay, following the same trend presented by the FWO method. Besides the significant difference between the calculated values for  $E_a$  and  $n$ , MLR allows to calculate the average activation entropy of the decomposition reaction:

$$\Delta S = 2.303 \left( \log \frac{A \cdot h}{T_{max} \cdot K} \right) R \quad (13)$$

where  $h$  and  $K$  are, respectively the Planck and Boltzmann constants [40]. The obtained values for  $\Delta S$  showed a small variation, ranging from  $-240.7 \text{ J}\cdot\text{mol}^{-1}$  (pure PP)

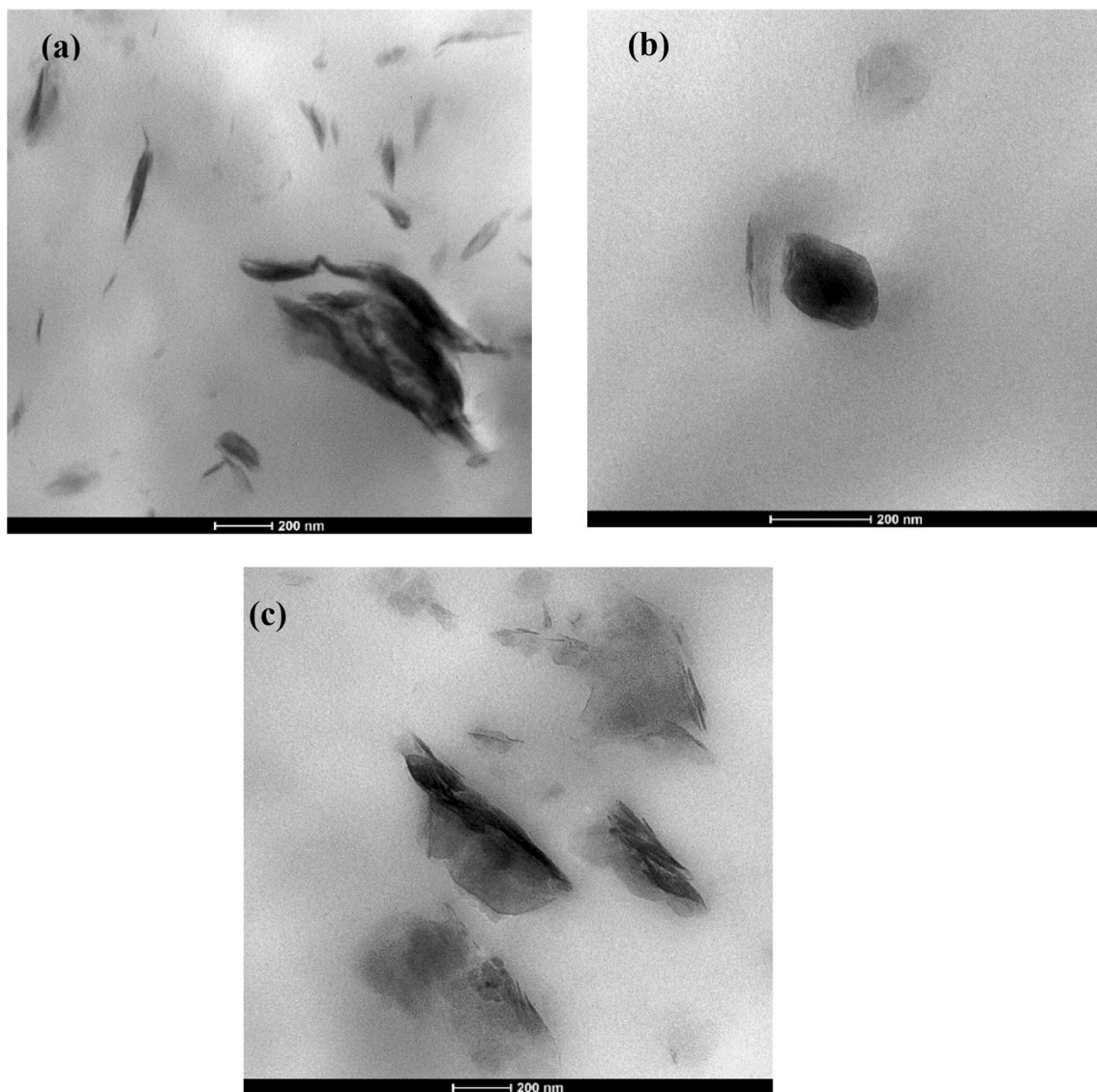


**Fig. 7** TEM micrographs of the PP nanocomposites containing [BMMIM]Cl in the compositions: **a** 1.5 wt%; **b** 3.0 wt% and **c** 5.0 wt%

to  $-244.9 \text{ J}\cdot\text{mol}^{-1}$  (5.0 wt% MMT-IL), corroborating the important role of the degree of intercalation/exfoliation on the activation energy. As a consequence, the thermal properties of polymer–clay nanocomposites based on IL as modifier for the clay mineral are strongly dependent not only of polymer–clay interactions but the internal morphology of the clay galleries.

The overall results obtained indicate that the use of short alkyl chain length imidazolium IL presents higher thermal stability when compared to the usual quaternary ammonium salt surfactant. Despite the elevated cost of the IL when compared to the quaternary ammonium surfactant, the use of these modifiers can contribute to process nanocomposites based on engineering polymers, as polyether ether ketone (PEEK) and polyimides (PI), whose processing temperatures are higher than the surfactant decomposition temperature range.

## 4 Conclusions

In this investigation, PP nanocomposites with imidazolium-based IL modified MMT were prepared and characterized for their thermal stability. The improvement in the thermal stability, accounted by the IPDT, was remarkable. Imidazolium-based modifiers showed IPDT values ranging 47–91 °C higher than the quaternary ammonium salts. The results indicate that the use of imidazolium-based IL with short alkyl chain length is promissory as organic modifier for lamellar clays instead the conventional quaternary ammonium salts.

In general, Flynn–Wall–Ozawa and MLR equations showed a decrease of  $E_a$  values to the nanocomposites comparing to the neat matrix. The activation energies calculated by these methods differ in their magnitude. However, it was observed that in both the methods, the activation energy increases with the percentage conversion. Therefore, the understanding of the IL thermal decomposition mechanisms and the way that these substances influence the thermal stability of the nanocomposites is

**Table 3** Thermal decomposition parameters obtained by MLR method at  $10 \text{ }^\circ\text{C}\cdot\text{min}^{-1}$  for PP/MMT-IL nanocomposites

Content of organoclay (wt%)	$E_a$ (kJ·mol <sup>-1</sup> )	Reaction order ( <i>n</i> )
0.0	397.64	1.05
1.5	248.05	0.32
3.0	438.12	0.50
5.0	105.60	0.68

The confidence limit was fixed in the range of  $\pm 5\%$

fundamental for the complete correlation between structure and property of the materials under analysis.

**Acknowledgements** The authors thank the São Paulo Research Foundation (FAPESP) for research grant (Grant 2011/12410-3).

**Authors' contribution** PV—Conceptualization, Formal analysis and investigation, Writing—original draft preparation. ACOG—Formal analysis and investigation. LMRO—Formal analysis and investigation. SAC—Formal analysis and investigation, Writing—review and editing. CMP—Conceptualization, Methodology, Formal analysis and investigation, Writing—review and editing, Supervision.

**Funding** São Paulo Research Foundation (FAPESP) for research grant (Grant 2011/12410-3).

**Data availability** The data that support the findings of the present manuscript are available from the corresponding author upon reasonable request.

**Declarations**

**Conflict of interest** The authors declare that they have no conflict of interest.

**Open Access** This article is licensed under a Creative Commons Attribution 4.0 International License, which permits use, sharing, adaptation, distribution and reproduction in any medium or format, as long as you give appropriate credit to the original author(s) and the source, provide a link to the Creative Commons licence, and indicate if changes were made. The images or other third party material in this article are included in the article's Creative Commons licence, unless indicated otherwise in a credit line to the material. If material is not included in the article's Creative Commons licence and your intended use is not permitted by statutory regulation or exceeds the permitted use, you will need to obtain permission directly from the copyright holder. To view a copy of this licence, visit <http://creativecommons.org/licenses/by/4.0/>.

## References

- Cheng S, Cairncross RA, Hsuan YG, Li CY (2013) Clay orientation effect on the thermal stability of polyethylene-nanoclay nanocomposites. *Polym* (United Kingdom). <https://doi.org/10.1016/j.polymer.2013.07.011>
- Le Pluart L, Duchet J, Sautereau H (2005) Epoxy/montmorillonite nanocomposites: influence of organophilic treatment on reactivity, morphology and fracture properties. *Polymer* (Guildf) 46:12267–12278. <https://doi.org/10.1016/j.polymer.2005.10.089>
- Livi S, Duchet-Rumeau J, Pham TN, Gérard J-F (2011) Synthesis and physical properties of new surfactants based on ionic liquids: Improvement of thermal stability and mechanical behaviour of high density polyethylene nanocomposites. *J Colloid Interface Sci* 354:555–562. <https://doi.org/10.1016/j.jcis.2010.10.058>
- Wang S, Song C, Chen G et al (2005) Characteristics and biodegradation properties of poly(3-hydroxybutyrate-co-3-hydroxyvalerate)/organophilic montmorillonite (PHBV/OMMT) nanocomposite. *Polym Degrad Stab* 87:69–76. <https://doi.org/10.1016/j.polymdegradstab.2004.07.008>
- Riechert V, Failla MD, Quinzani LM (2017) Effect of montmorillonite on the crystallization and thermal degradation of poly(propylene-co-ethylene-co-1-butene) nanocomposites.

- J Thermoplast Compos Mater 30:741–761. <https://doi.org/10.1177/0892705715610409>
6. Koo J (2006) Polymer nanocomposites: processing, characterization, and applications, 1st edn. New York, McGraw-Hill Education
  7. Sinha Ray S, Okamoto M (2003) Polymer/layered silicate nanocomposites: a review from preparation to processing. *Prog Polym Sci* 28:1539–1641. <https://doi.org/10.1016/j.progpolymsci.2003.08.002>
  8. Ding Y, Guo C, Dong J-Y, Wang Z (2006) Novel organic modification of montmorillonite in hydrocarbon solvent using ionic liquid-type surfactant for the preparation of polyolefin–clay nanocomposites. *J Appl Polym Sci* 102:4314–4320. <https://doi.org/10.1002/app.24904>
  9. He A, Wang L, Yao W et al (2010) Structural design of imidazolium and its application in PP/montmorillonite nanocomposites. *Polym Degrad Stab* 95:651–655. <https://doi.org/10.1016/j.polymdegradstab.2009.12.003>
  10. Kim NH, Malhotra SV, Xanthos M (2006) Modification of cationic nanoclays with ionic liquids. *Microporous Mesoporous Mater* 96:29–35. <https://doi.org/10.1016/j.micromeso.2006.06.017>
  11. Kim S, Park S-J (2009) Interlayer spacing effect of alkylammonium-modified montmorillonite on conducting and mechanical behaviors of polymer composite electrolytes. *J Colloid Interface Sci* 332:145–150. <https://doi.org/10.1016/j.jcis.2008.12.006>
  12. Xie W, Gao Z, Pan W-P et al (2001) Thermal degradation chemistry of alkyl quaternary ammonium montmorillonite. *Chem Mater* 13:2979–2990. <https://doi.org/10.1021/cm010305s>
  13. Zhang Q, Fu Q, Jiang L, Lei Y (2000) Preparation and properties of polypropylene/montmorillonite layered nanocomposites. *Polym Int* 49:1561–1564
  14. Awad WH, Gilman JW, Nyden M et al (2004) Thermal degradation studies of alkyl-imidazolium salts and their application in nanocomposites. *Thermochim Acta* 409:3–11. [https://doi.org/10.1016/S0040-6031\(03\)00334-4](https://doi.org/10.1016/S0040-6031(03)00334-4)
  15. Goswami SK, Ghosh S, Mathias LJ (2012) Thermally stable organically modified layered silicates based on alkyl imidazolium salts. *J Colloid Interface Sci* 368:366–371. <https://doi.org/10.1016/j.jcis.2011.11.032>
  16. Barbosa R, Araújo EM, de Oliveira AD, de Melo TJA (2006) Efeito de sais quaternários de amônio na organoflização de uma argila bentonita nacional. *Cerâmica* 52:264–268. <https://doi.org/10.1590/S0366-69132006000400009>
  17. Ngo HL, LeCompte K, Hargens L, McEwen AB (2000) Thermal properties of imidazolium ionic liquids. *Thermochim Acta* 357–358:97–102. [https://doi.org/10.1016/S0040-6031\(00\)00373-7](https://doi.org/10.1016/S0040-6031(00)00373-7)
  18. Zhu J, Morgan AB, Lamelas FJ, Wilkie C (2001) Fire properties of polystyrene-clay nanocomposites. *Chem Mater* 13:3774–3780. <https://doi.org/10.1021/cm000984r>
  19. Cui L, Bara JE, Brun Y et al (2009) Polyamide- and polycarbonate-based nanocomposites prepared from thermally stable imidazolium organoclay. *Polymer (Guildf)* 50:2492–2502. <https://doi.org/10.1016/j.polymer.2009.03.036>
  20. Cammarata L, Kazarian SG, Salter PA, Welton T (2001) Molecular states of water in room temperature ionic liquids electronic supplementary information available. See <http://www.rsc.org/suppdata/cp/b1/b106900d/>. *Phys Chem Chem Phys* 3:5192–5200. <https://doi.org/https://doi.org/10.1039/b106900d>
  21. Dupont J, Consorti CS, Suarez PAZ et al (2002) Preparation of 1-butyl-3-methyl imidazolium-based room temperature ionic liquids. *Org Synth* 79:236. <https://doi.org/10.15227/orgsyn.079.0236>
  22. Xu A, Wang J, Wang H (2010) Effects of anionic structure and lithium salts addition on the dissolution of cellulose in 1-butyl-3-methylimidazolium-based ionic liquid solvent systems. *Green Chem* 12:268–275. <https://doi.org/10.1039/B916882F>
  23. Kim NH (2006) Modification of clays with ionic liquids for polymer nanocomposites. New Jersey Institute of Technology, New Jersey
  24. Shah KJ, Mishra MK, Shukla AD et al (2013) Controlling wettability and hydrophobicity of organoclays modified with quaternary ammonium surfactants. *J Colloid Interface Sci* 407:493–499. <https://doi.org/10.1016/j.jcis.2013.05.050>
  25. de Lima JA, Fitaroni LB, Chiaretti DV et al (2017) Degradation process of low molar mass poly(ethylene terephthalate)/organically modified montmorillonite nanocomposites. *J Thermoplast Compos Mater* 30:504–520. <https://doi.org/10.1177/0892705715604678>
  26. Vaslova M, Dominguez-Patiño G, Kakazey N et al (2003) Structural-phase transformations in bentonite after acid treatment. *Sci Sinter* 35:155–166. <https://doi.org/10.2298/SOS0303155V>
  27. Fitaroni LB, de Lima JA, Cruz SA, Waldman WR (2016) Effect of compatibilizer and Irganox MD 1024 on the thermo-oxidative stability of PP/PP-g-MA/OMMT nanocomposites. *Polym Test* 53:165–173. <https://doi.org/10.1016/j.polymertesting.2016.05.016>
  28. Doyle CD (1961) Estimating thermal stability of experimental polymers by empirical thermogravimetric analysis. *Anal Chem* 33:77–79. <https://doi.org/10.1021/ac60169a022>
  29. Ozawa T (1965) A new method of analyzing thermogravimetric data. *Bull Chem Soc Jpn* 38:1881–1886. <https://doi.org/10.1246/bcsj.38.1881>
  30. Flynn JH, Wall LA (1966) General treatment of the thermogravimetry of polymers. *J Res Natl Bur Stand Sect A Phys Chem* 70A:487. <https://doi.org/10.6028/jres.070A.043>
  31. Arda B, Bal A, Acar I (2017) Characterization of the thermal oxidative degradation kinetics of thermoplastics. *Instrum Sci Technol* 45:558–576. <https://doi.org/10.1080/10739149.2017.1278705>
  32. Aboulkas A, El harfi K, El Bouadili A (2010) Thermal degradation behaviors of polyethylene and polypropylene. Part I: pyrolysis kinetics and mechanisms. *Energy Convers Manag* 51:1363–1369. <https://doi.org/10.1016/j.enconman.2009.12.017>
  33. Carrasco F, Pagès P, Gámez-Pérez J et al (2010) Kinetics of the thermal decomposition of processed poly(lactic acid). *Polym Degrad Stab* 95:2508–2514. <https://doi.org/10.1016/j.polymdegradstab.2010.07.039>
  34. Nisar J, Khan MA, Iqbal M et al (2016) Comparative study of kinetics of the thermal decomposition of polypropylene using different methods. *Adv Polym Technol*. <https://doi.org/10.1002/adv.21776>
  35. Widmann G (1982) Kinetic measurements on polymers: applications and limits. *J Therm Anal* 25:45–55. <https://doi.org/10.1007/BF01913053>
  36. Chan JH, Balke ST (1997) The thermal degradation kinetics of polypropylene: Part III. Thermogravimetric analyses *Polym Degrad Stab* 57:135–149. [https://doi.org/10.1016/S0141-3910\(96\)00160-7](https://doi.org/10.1016/S0141-3910(96)00160-7)
  37. Snegirev AY, Talalov VA, Stepanov VV et al (2017) Autocatalysis in thermal decomposition of polymers. *Polym Degrad Stab* 137:151–161. <https://doi.org/10.1016/j.polymdegradstab.2017.01.008>
  38. Peterson JD, Vyazovkin S, Wight CA (2001) Kinetics of the thermal and thermo-oxidative degradation of polystyrene, polyethylene and poly(propylene). *Macromol Chem Phys* 202:775–784. [https://doi.org/10.1002/1521-3935\(20010301\)202:6%3c775::AID-MACP775%3e3.0.CO;2-G](https://doi.org/10.1002/1521-3935(20010301)202:6%3c775::AID-MACP775%3e3.0.CO;2-G)
  39. Marini F, Tomassetti M, Vecchio S (2012) Detailed kinetic and chemometric study of the cellulose thermal breakdown in artificially aged and non aged commercial paper. Different methods for computing activation energy as an assessment model in archaeometric applications. *Chem Cent J*. <https://doi.org/10.1186/1752-153X-6-52-57>

40. Yakuphanoglu F, Gorgulu AO, Cukurovali A (2004) An organic semiconductor and conduction mechanism: N-[5-methyl-1,3,4-tiyodiazole-2-yl] ditiyocarbamate compound. *Phys B Condens Matter* 353:223–229. <https://doi.org/10.1016/j.physb.2004.09.099>

**Publisher's Note** Springer Nature remains neutral with regard to jurisdictional claims in published maps and institutional affiliations.